Phys. Chem. Glasses, 2001, **42** (3), 191–8

Isothermal sintering with concurrent crystallisation of monodispersed and polydispersed glass particles. Part 1

E. D. Zanotto[1] *& M. O. Prado*[2]

Vitreous Materials Laboratory, Department of Materials Engineering, Federal University of São Carlos, CP 676, CEP 13.565-905 São Carlos, SP, Brazil

We review and discuss an algorithm with no adjustable parameters to simulate the kinetics of concurrent sintering and crystallisation of monodispersed and polydispersed glass particles. The algorithm is based on the two classical sintering models of Frenkel and Mackenzie–Shuttleworth, the JMAK crystallisation theory and on our own model for polydispersed particle sintering. The input parameters are: particle size distribution (v_r), surface tension (γ), viscosity (η), number of nucleation sites (N_s) and crystal growth velocity (U). We test the algorithm at a variety of annealing temperatures using experimental data and densification rates for two powdered glasses–polydispersed alumino-borosilicate glass, which is stable against devitrification, and monodispersed cordierite glass which easily crystallises. We show that the algorithm provides a powerful simulation tool for predicting the sintering conditions of real glass powders, for any size distribution and temperature, thus minimising the number of time consuming experiments.

The preparation of glass articles by sintering is well established laboratory and industrial practice.[1] Recently, however, the development of advanced materials by sintering, e.g. sintered glass ceramics, sol-gel derived glasses, amorphous and crystalline thin films and novel metallic alloys, has reawakened the need for a deeper understanding and tighter control of processing parameters to avoid spontaneous crystallisation (which hinders viscous flow sintering) and residual porosity in such materials.

Several models have been proposed and many experiments conducted on viscous flow sintering. Models that predict the isothermal densification of a porous body, composed of glass particles having the same size or porous compacts having identical pores, successfully describe parts of the sintering process.[2,3]

Just to mention a few models that are relevant to this study, Giess *et al*[2] reported that the Mackenzie–Shuttleworth analysis does not accurately describe the sintering of pressed compacts of polydispersed, irregular shaped glass particles, suggesting that this drawback may be the result of smaller particle size fractions sintering more rapidly than the larger ones. Numerical simulation has been applied to viscous sintering to study pore size distribution during sol-gel processing.[4] Exner *et al*[5] developed a stereological model to describe the shrinkage in sintering polydispersed glass powders. To our knowledge, however, very few attempts[6,7] have been made to describe the sintering kinetics of real glass powders that undergo concurrent devitrification. Thus the objective of this paper is to review and test an algorithm that considers sintering with simultaneous crystallisation under isothermal conditions.

We begin by presenting the classical Frenkel (F) and Mackenzie–Shuttleworth (MS) models for the sintering of spherical monodispersed glass particles. We then review our clustering model for the sintering of a particle size distribution, introduce the problem of concurrent crystallisation (that hinders sintering) and derive the densification equations. Next we test the equations with a stable (nondevitrifying) composition—an alumino-borosilicate glass—as well as with an easily crystallisable glass—stoichiometric cordierite. We follow this with a discussion of the results of our tests and some important drawbacks of the models such as the influence of irregular particle shape, shrinkage anisotropy, temperature gradients within the samples, internal crystallisation and residual porosity. Finally, we discuss the processing parameters that control the regions where sintering is most favourable over crystallisation—the working windows. In Part 2 of this paper[8] we extend the algorithm for nonisothermal conditions.

Summary of the theory

Frenkel and Mackenzie–Shuttleworth models

The Frenkel model, Equations (1a) and (1b) offers a good description of the isotropic sintering of monodispersed spherical particles.[9] Starting from a compact consisting of loosely packed powder with a relative density of about 0·6, the model works up to a relative density of $\rho=\rho(t)/\rho_g \approx 0{\cdot}8$ (where $\rho(t)$ is the bulk density of the compact and

[1] Author to whom correspondence should be addressed. (e-mail: dedz@power.ufscar.br)
[2] On leave from the Comisión Nacional de Energía Atómica, Centro Atómico Bariloche, 8400- SC de Bariloche, Argentina

ρ_g the glass density) or, equivalently, up to a linear shrinkage of approximately 10%

$$\frac{\Delta L}{L_0} = \frac{3\gamma}{8\eta(T)r}t \tag{1a}$$

Equation (1a) can be rewritten in terms of the relative densities

$$\frac{\rho(t)}{\rho_0} = \left(1 - \frac{3\gamma t}{\eta(T)r}\right)^{-3} \tag{1b}$$

where L_0 is the original sample length, ΔL the linear shrinkage after a sintering time t, $\eta(T)$ the temperature dependent shear viscosity, γ the glass vapour surface energy (whose dependence on temperature is very slight), r the initial particle radius and ρ_0 the initial density of the compact.

For higher relative densities, when spherical pores are isolated in the glass, the Mackenzie–Shuttleworth, MS model gives the following densification rate.[3,10]

$$\frac{d\rho}{dt} = \frac{3\gamma}{2a_0\eta(T)}(1-\rho) \tag{2}$$

where a_0 is the initial radius of the spherical pores. Equation (2) is presented in a simplified way that allows for a simple mathematical treatment.[3] Actually we approximate $(1-\rho)/a$ by $(1-\rho)/a_0$ where a is the pore radius, which is assumed to shrink, while the pore number remains fixed.

These two models describe well the isothermal densification of glass.[11,12]

On a laboratory time scale sintering is only accomplished at temperatures above that of glass transition, T_g, with the viscosity curve $\eta(T)$ normally described by the Vogel–Fulcher–Tamman (VFT) equation[13]

$$\eta = \eta_\infty e^{\frac{E_v}{R(T-T_0)}} \tag{3}$$

where R is the gas constant, T_o an empirical constant, E_v an apparent activation energy associated to molecular transport by viscous flow, and η_∞ the viscosity at an 'infinite' temperature. T_o, E_v and η_0 are empirically obtained from shear viscosity measurements. In this paper we use measured values of viscosity as an input parameter in the simulations.

Clustering model. Glass densification with a particle size distribution

Previous studies have demonstrated that the F model describes the initial stage and the MS model describes the final stage of sintering of monodispersed spherical particles.[11,12] However, the situation of real powders having a size distribution is more complex.

Figure 1(a, b) show SEM images of a compact of polydispersed particles after a linear shrinkage of about 8%. Although the largest particles are clearly at the (initial) Frenkel stage, which is characterised by the formation of a neck between neighbouring particles, the smaller particles (having a higher specific surface area

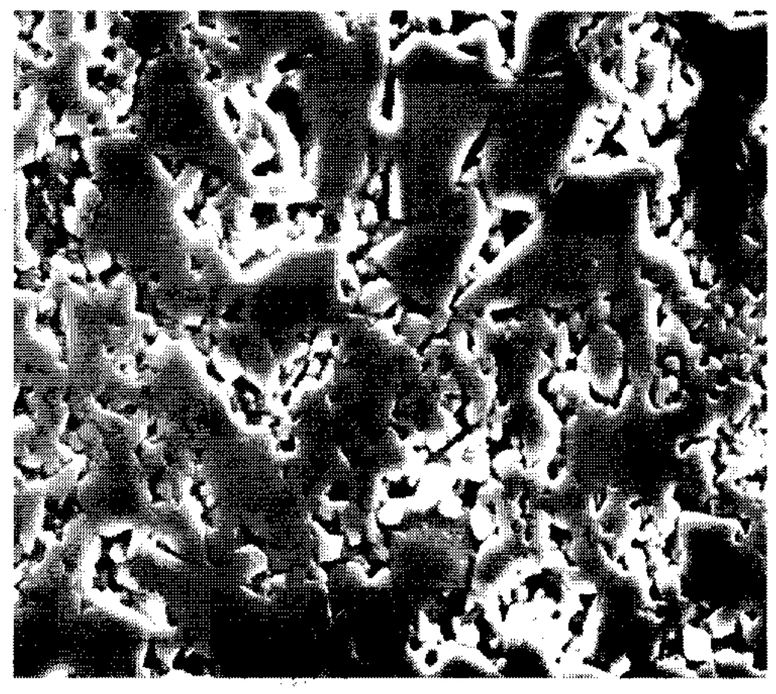

(a)

(b)

Figure 1. *SEM micrographs of a polydispersed compact after a linear shrinkage of 8%. Magnification: (a)×1200; (b) ×5000. (b) gray arrows: small sintered particles; white arrow: neck between two large particles; dashed white arrow: neck between a compact of small particles and a large particle*

and thus a higher driving force for sintering) have already overcome this stage. This was the basis for the model previously proposed by the present authors:[14] small particles preferentially cluster in the open spaces left by larger particles and sinter faster. Thus, for a polydispersed compact with volume fraction v_r of particles of radius r, the following expression holds true for the densification kinetics at a given temperature.

$$\rho(t) = \sum_r \left[\rho_F(r,t)\theta_F(t_{0\cdot8}-t)\xi_r + \rho_{MS}(r,t)\theta_{MS}(t-t_{0\cdot8})\right]\frac{v_r}{N}$$

$$N = \sum_r \left[\theta_F(t_{0\cdot8}-t)\xi_r + \theta_{MS}(t-t_{0\cdot8})\right] \tag{4}$$

Equation (4) sums up the relative density $\rho(r,t)$ for each particle size, r, as a function of time, t. During the Frenkel stage of sintering, the $\rho(r,t)<0{\cdot}8$ condition is met and $\rho_F(r,t)$ is calculated using the Frenkel equation, Equation (1b). Later, $\rho(r,t)>0{\cdot}8$, $\rho_{MS}(r,t)$ is calculated by the Mackenzie–Shuttleworth model, Equation (2).[6] For each cluster the passage from the Frenkel regime to the MS regime is performed using the step

In Equation (4) ξ_r only multiplies the Frenckel part of sintering while, in the previous version, ξ_r multiplies both stages of sintering.

functions $\theta_F(t_{0.8}-t)$ and $\theta_{MS}(t-t_{0.8})$, whose values switch between 1 and 0 at $t=t_{0.8}$ when $\rho_F(r,t_{0.8})=0{\cdot}8$ is reached. Thus, $\theta_F(t_{0.8}-t)=1$ and $\theta_{MS}(t-t_{0.8})=0$ for $t<t_{0.8}$ and $\theta_F(t_{0.8}-t)=0$ and $\theta_{MS}(t-t_{0.8})=1$ for $t>t_{0.8}$. ξ is the neck forming ability of each particle which can be calculated from the particle size distribution.[14] Thus, the model does not rely on any adjustable parameter.

The pore radius a_0 in Equation (2) was adjusted to guarantee a continuous $\rho(r,t)$ function at $t=t_{0.8}$. The adjustment was achieved by first computing $t_{0.8}$ with Equation (1b) then calculating a_0 with the integrated version of Equation (2) at $t=t_{0.8}$.

Equation (4) can be explicitly written as

$$\rho(t)=\sum_r\left(\frac{\dfrac{\rho_0}{\rho_g\left(1-\dfrac{3\gamma t}{8\eta(T)r}\right)^3}\theta(t_{0.8}-t)\xi_r}{+\left(1-e^{\left(\frac{-3\gamma t}{2a_0(r)\eta(T)}+\ln\left(1-\frac{\rho_0}{\rho_g}\right)\right)}\right)\theta(t-t_{0.8})}\right)\frac{v_r}{N} \quad (5)$$

To test the proposed model we used a polydispersed, irregular shaped borosilicate glass powder (that was stable against crystallisation) and determined the densities of uniaxially die pressed cylindrical samples by weighing and measuring their diameters and heights after sequential isothermal heat treatments. The relative densification rate ($\partial\rho/\partial t$) was obtained from both linear shrinkage and buoyancy measurements as a function of time for various sintering temperatures. A corrected sintering time was introduced to allow for the retarded thermal equilibrium in the sample interior. In all the stages of sintering, $\ln(\partial\rho/\partial t)$ showed a linear dependence on $(T-T_o)^{-1}$, Equations (1)–(3), indicating a process controlled by viscous flow as we had expected. However, we found a marked sintering anisotropy ascribed to particle orientation and preferential compaction during pressing. The sintering curves at different temperatures followed a unique 'master curve' when plotted against the reduced time $\gamma t/\eta$. The full experimental procedures and testing of the clustering model are described in detail in Ref. 14. The clustering model provided a good description of the sintering kinetics of this polydispersed noncrystallising powder.

When dealing with monodispersed particles, Equations (4)–(5) hold true if one equates the product $v_r\xi$ to unity and eliminates the $\sum_r$ sum.

Isothermal sintering with concurrent crystallisation

Most glass powders have a tendency to crystallise starting from the external surfaces when heated[15] and any fraction of the surface that crystallises hinders sintering by preventing viscous flow. It is, therefore, important to understand the effect of surface crystallisation on the sintering kinetics. This subject will be discussed in the following section, following a more elaborate presentation.[16]

For powdered glasses we assume the most typical case of heterogeneous nucleation of spherical crystals growing with a linear growth rate $U(T)$ from a fixed number of sites per unit area, N_s. In this case the JMAK[17] theory predicts the surface fraction crystallised, α_s

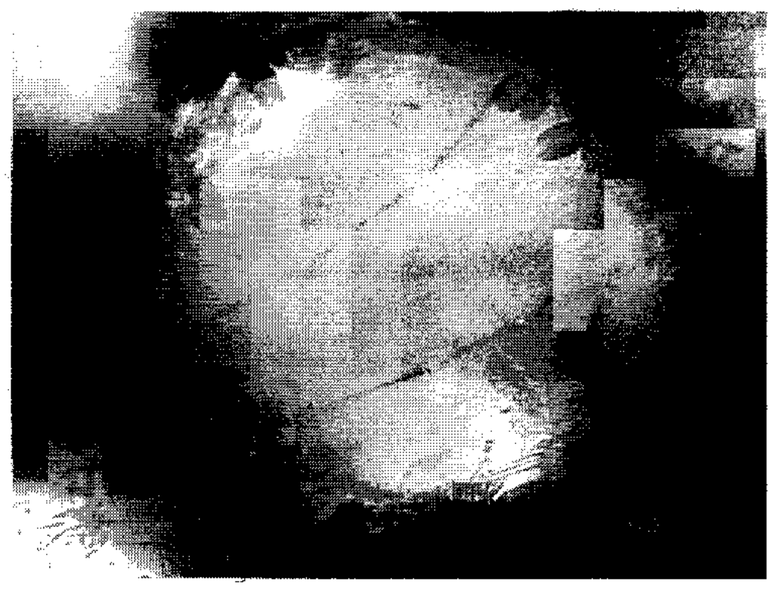

Figure 2. *Crystals growing from the surface towards the volume of a spherical soda–lime–silica glass particle in a sintering crystallisation experiment. Necks between particles are clearly shown*

$$\alpha_s=1-e^{\left(-\pi N_s U(T)^2 t^2\right)} \quad (6)$$

where t is the time of isothermal treatment.

Müller[18] reasonably assumed that, regardless of the sintering model, the densification rate should decrease in proportion to the surface fraction of glass remaining after crystallisation. Hence, in this case, the isothermal densification rate is

$$\frac{d\rho_c}{dt}=\frac{d\rho}{dt}(1-\alpha_s) \quad (7)$$

where ρ_c is the relative density of a compact that partially devitrifies during sintering.

Inserting the appropriate expressions for $d\rho/dt$ (from Equations (1b) and (2)) and α_s (Equation (6)) into Equation (7), upon integration one arrives at Equations (8) and (9) for the Frenkel and Mackenzie–Shuttleworth cases, respectively

$$\rho_{c,F}(t)=\rho_0+\frac{9\gamma p_0}{8r\eta(T)}\int_0^t\left(1-\frac{3\gamma}{8r\eta(T)}t'\right)^{-4}e^{-\pi N_s U(T)^2 t'^2}dt' \quad (8)$$

$$\rho_{c,MS}(t)=\rho_0+(1-\rho_0)\frac{3\gamma}{2a_0\eta(T)}\int_0^t e^{-\frac{3\gamma t'}{2a_0\eta(T)}}e^{-\pi N_s U(T)^2 t'^2}dt' \quad (9)$$

With these equations and the appropriate physical parameters of the glass (surface tension, viscosity, crystal growth rate versus temperature, number of active surface sites, particle size distribution and green density) it is possible to predict the densification kinetics (ρ or ρ_c versus time) at any chosen temperature. With the exception of $U(T)$, which must be measured, the other parameters can be estimated from the glass composition (η, γ) or be used as simulation parameters (N_s, r, ρ_0). Equations (8) and (9) can easily be extended to the case where more than one crystalline phase forms. By introducing Equations (8) and (9) into Equation (5), polydispersed distributions undergoing sintering and concurrent crystallisation can be treated.

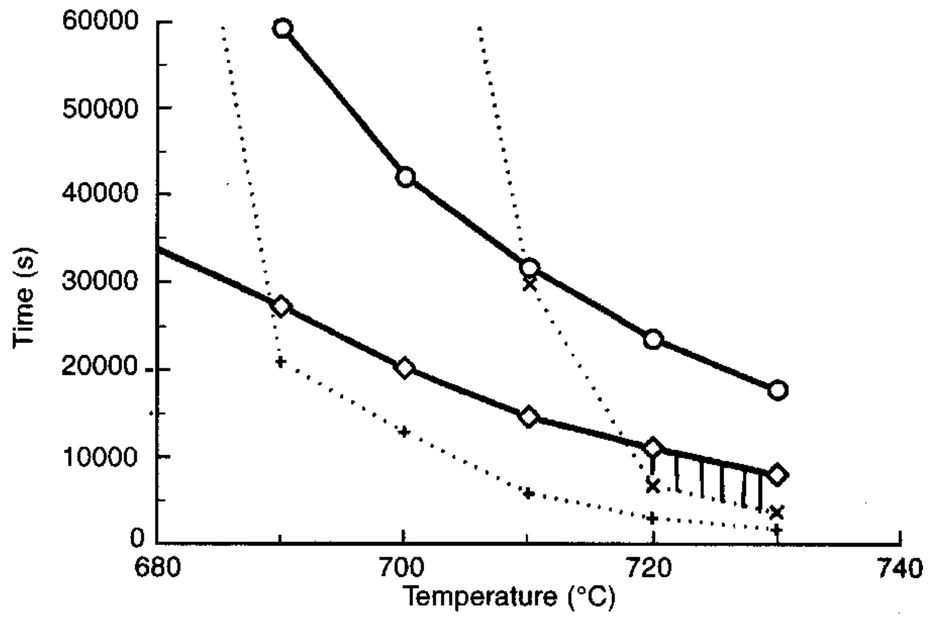

Figure 3. T–t–ρ–α *plot for a spherical particle of soda–lime–silica glass [16]. Dashed* T–t *region where* $\rho>0{\cdot}99$ *and* $\alpha_V<0{\cdot}001$. *This region lies at temperatures above the softening temperature* $T_{soft}=704°C$
+ $\rho_c=0{\cdot}975$ × $\rho_c=0{\cdot}99$ ◇ $\alpha_v=0{\cdot}001$ ○ $\alpha_v=0{\cdot}01$

Crystallisation towards the volume

Figure 2 shows a spherical particle of soda–lime–silica glass that formed necks during sintering and whose surface is fully crystallised (cristobalite and devitrite), with crystals growing from the surface towards the interior of the particle. In this case crystallisation stopped sintering.

Crystals nucleated at the surface of the particle not only cover this surface but also grow towards the particle's core. Gutzow[19] described the kinetics of this volume transformation for spherical crystals. Before the growing crystals begin to interact, the volume crystallisation kinetics is a function of t^3 but when they impinge the kinetics of volume crystallisation is proportional to t^1. Equations (12a) and (12b) hold true in each case for each crystalline phase p.

$$\alpha^{p}_{v,r} = 1 - e^{-\frac{N_p 2\pi U_p^3 t^3}{r}} \qquad t < 0.5/\left(N_p U_p^2\right)^{1/2} \qquad (10a)$$

$$\alpha^{p}_{v,r} = 1 - e^{-\frac{3N_p \pi d_0^2 U_p t}{4r}} \qquad t > 0.5/\left(N_p U_p^2\right)^{1/2} \qquad (10b)$$

In Equations (10a) and (10b) the superscript p indicates a given crystalline phase and the subscripts v and r indicate volume crystallisation and particle radius, respectively.

Working windows

*Temperature–time–isodensity–isocrystallised fraction (*T–t–ρ–α*) graphs.* If the model is able to consider concurrent surface and volume crystallisation during sintering[16] it allows one to calculate the appropriate thermal treatment (time and temperature) in order to obtain the desired porosity and crystallinity of the compact. Based on the particle size distribution, η, γ, ρ_o, ρ_g, N_p and U_p, $\rho(t)$ curves can then be calculated at different temperatures using Equation (5). These curves take into account the effect of surface crystallisation on sintering, as discussed in the section *Isothermal sintering with concurrent crystallisation.* Curves of the crystallised volume for each phase, $\alpha_V(t)$, can be calculated at different temperatures using Equations (10a) and (10b).

Difficulties may arise in determining N_p if the particle surface is not smooth and also when the crystal geometry is other than spherical. For example, calculations related to needle shaped crystals (such as devitrite) must be confirmed by experimental XRD results of the crystallised volume. From those curves, iso-ρ and iso-α_V lines can be plotted on a T–t (temperature–time) diagram (Figure 3).

The curve $\rho=0{\cdot}9$ in Figure 3 divides the T–t plane into two regions. The region corresponding to higher times corresponds to densities exceeding 0·9. The curve $\alpha_V(t)=0{\cdot}001$ also divides the T–t plane into two regions. The descending (T,t) points correspond to times for which $\alpha_V(t)<0{\cdot}001$. Thus, the intersection of these semi-planes determines a working window where ρ is higher and α_V is lower than certain desired values. T–t sectors such as the dashed one shown in Figure 3, calculated for a polydispersed distribution of soda–lime–silica glass spheres with average radius around 200 microns, can be determined where desired conditions of density and crystallinity can be achieved.

Results: testing the equations with real glasses

Isothermal sintering of alumino-borosilicate glass

An alumino-borosilicate glass of composition (wt%) $71{\cdot}70SiO_2$, $8{\cdot}33B_2O_3$, $8{\cdot}56Al_2O_3$, $1{\cdot}00MgO$, $2{\cdot}67CaO$, $7{\cdot}44Na_2O$, which is a candidate for nuclear waste encapsulation, was used owing to its stability against devitrification and resistance to water corrosion.[20,21] This is convenient for our studies because the original surface and number of nucleation sites remained unchanged during the experimental period. Therefore, this glass was used not only because its sintering behaviour is technologically significant but also to test the clustering model.

The glass transition temperature, $T_g^{DSC}\approx845$ K was determined by differential scanning calorimetry at 10 K/min. Figure 4 shows the particle size distribution measured with a Mastersizer μ Ver.2. High temperature viscosity measurements were taken using a rotating cylinder and a penetration viscometer. The viscosity showed a Vogel–Fulcher–Tamman behaviour with $\eta_\infty=e^{-4{\cdot}8026}$ Pa s, $E_v=95{\cdot}35$ kJ/mol and $T_0=510{\cdot}54$ K.

The glass vapour surface energy γ varies slightly with temperature but there are no data available for our glass at temperatures near T_g at which the sintering experi-

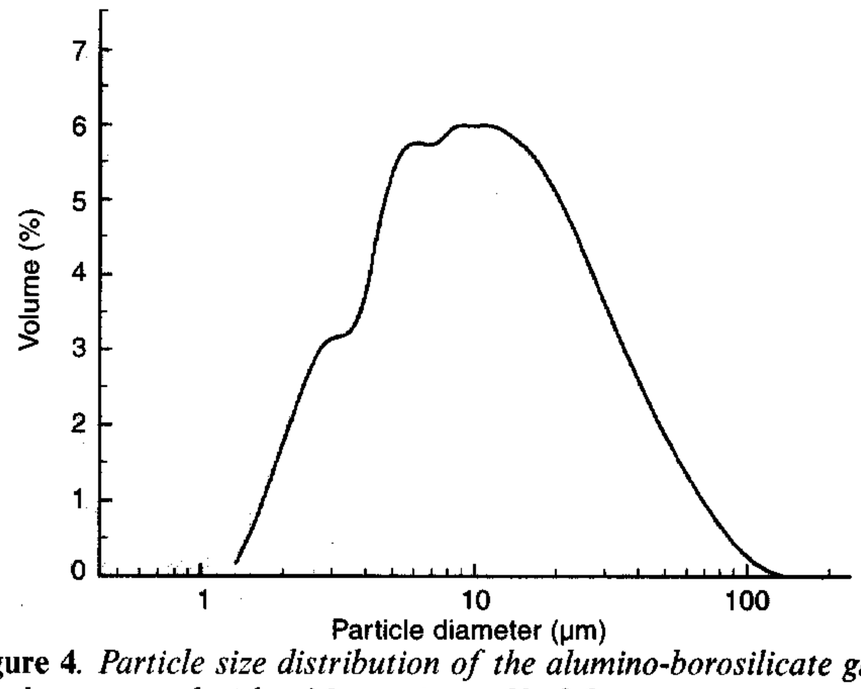

Figure 4. *Particle size distribution of the alumino-borosilicate glass powder measured with a Mastersizer μ Ver.2.0*

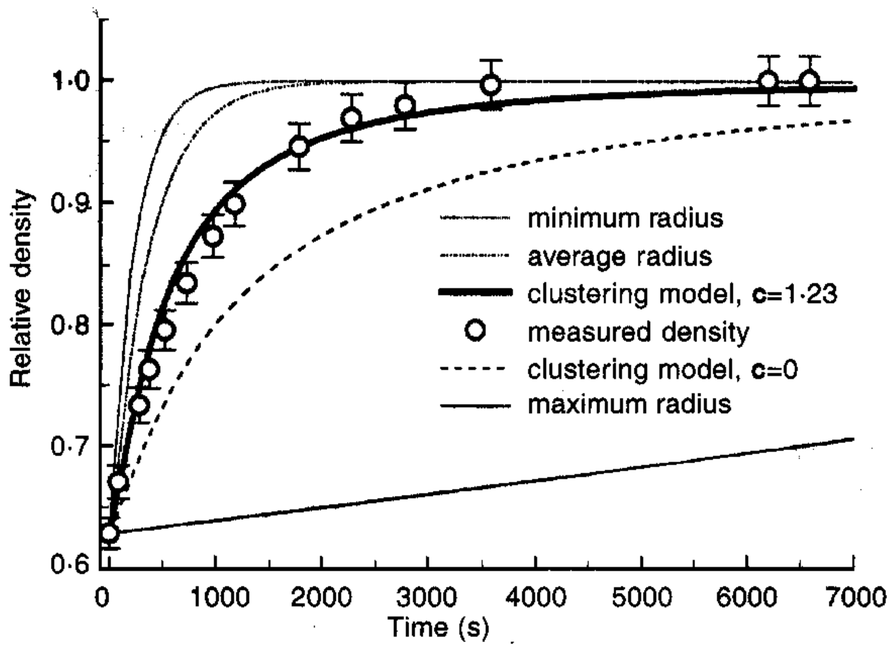

Figure 5. *Relative density versus time at 989 K for the alumino-borosilicate glass showing the sintering kinetics of: (a) smallest particles; (b) average particles; (c) clustering model with* c=*1·23; (d) clustering model with* c=*0 ; (e) largest particles of the distribution* $\xi_r=(1/r^2)/\Sigma_r(v_i/r^c)$

ments were performed. Hence, extrapolated data were used employing Lyon's method.[22] The values of γ extend from 0·327 J/m^2 at 959 K to 0·325 J/m^2 at 1017 K.

Cylindrical powder compacts were prepared by uniaxial die pressing of around 0·75 g of sample glass powder at 0·5 MPa for 30 s. The cylinders were approximately 6 mm high and 10·2 mm in diameter. The sample length, l, and diameter, ϕ, were measured after each sequential isothermal sintering step to determine the relative density. When the density stopped increasing with heat treatment, the final compact density was determined by the Archimedes method using liquid mercury.

The fact that the samples did not reach thermal equilibrium instantaneously when brought to the sintering temperature was considered. The corrections performed are detailed in Ref. 14.

To gain a better understanding of the real sintering process we calculated the sintering curves of idealised monodispersed powders together with the calculation corresponding to the real particle size distribution. Figure 5 shows the calculated sintering curves for a monodispersed distribution of the smallest particles, for the average particle size and for the largest particles of the measured particle size distribution. The curves corresponding to the polydispersed distribution were calculated using the clustering model with c=1·23 and 0. A comparison of the kinetics of these idealised processes with the real one highlights the effect of having a polydispersed distribution. The sintering kinetics of the real distribution is close to that of the average particles.

Due to the pressure of the entrapped gases in the closed pores (discussed later in this article) our samples never reached full density, ρ=1, but only ρ_f=0·96 at the final stage of sintering. This final density was used throughout our calculations instead of ρ_g.

Stoichiometric cordierite glass

In 1990, Technical Committee 7 (TC-7) of the International Commission on Glass started an extensive cooperative program to advance the understanding of surface nucleation and crystallisation phenomena. The crystallisation of metastable high quartz solid solution

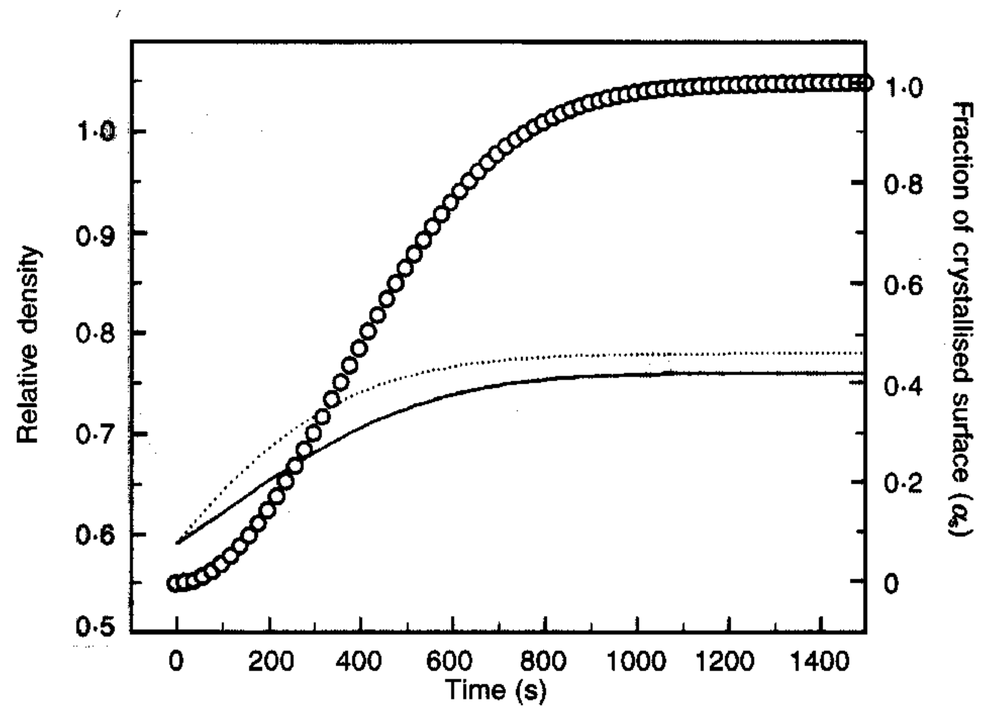

Figure 6 *Calculated sintering kinetics of spherical cordierite particles* r=10^{-5} *m at 1200°C according to the Frenkel and MS models, including surface crystallisation. The crystallised surface fraction is shown* ○ α_s — Frenkel ····· MS

crystals (μ-cordierite) and 'X-phase' crystals (both of cordierite composition $2MgO–2Al_2O_3–5SiO_2$) in cordierite glass were chosen as model cases. This choice was mainly due to the high chemical durability of cordierite glass, its polymorphic course of crystallisation and the absence of volume crystallisation.[23–5]

In the course of their studies various research groups observed that, for most thermal paths and size distributions, stoichiometric or near stoichiometric cordierite powders crystallised before reaching significant densification.[6] In this paper, therefore, we make use of the equations previously derived and test the sintering versus crystallisation competition for a range of particle sizes and annealing temperatures. We will show that the models correctly predict the observed behaviour (easy crystallisation and hence difficult densification).

For example the densification and surface crystallisation curves in Figure 6 were calculated using the experimental viscosity $\eta(T)$ in the form predicted by Equation (11), the crystal growth velocity $U(T)$ given by Equation (12) which is valid in the range of temperatures used, particle size r=10^{-5} m, initial relative density ρ_0=0·59, glass vapour surface tension γ=0·36 J/m^2 and crystal nucleus density N_S=10^{10} m^{-2} (typical for ground powders)

$$\eta(T)=e^{2\cdot3026\left(-7\cdot83+\frac{9488\cdot5}{T-596\cdot4}\right)} \tag{11}$$

$$U(T)=e^{-\frac{73331}{T}+42\cdot81} \tag{12}$$

with $\eta(T)$ in Pa s. , T in K and $U(T)$ in m/s.

Figure 6 shows that the compact density never reaches the MS state (ρ=0·8) since surface crystallisation precludes full densification.

Discussion

Alumino-borosilicate glass

The superimposition of all the sintering curves within experimental error when plotted against the corrected reduced time $\gamma t/\eta$ (Figure 7) confirms the absence of surface crystallisation of the powder and sintering con-

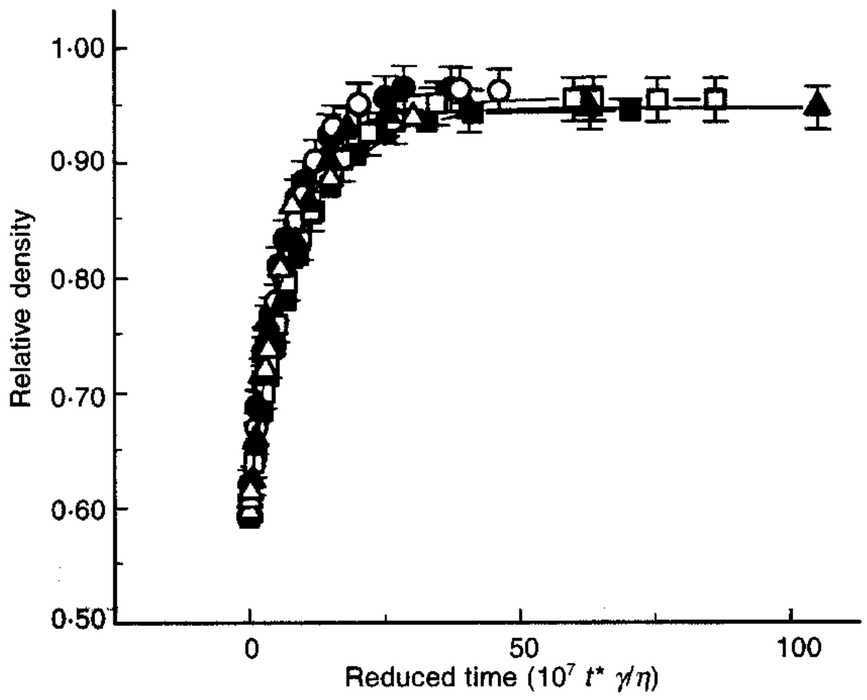

Figure 7. *Sintering curves at 959, 966, 980, 989, 999 and 1017 K as a function of reduced time 10^7 $\gamma t^*/\eta$*
● 959 K ○ 966 K ■ 980 K □ 989 K ▲ 999 K △ 1017 K

trolled by viscous flow. It also provides a test for the accuracy of our time, temperature and density measurements.

The cluster model, Equation (5), is a natural way of expressing the sintering of a polydispersed distribution of particles based on the simplest existing models (F & MS). Because clusters of small particles sinter faster than larger particle clusters, the model allows for regions of Frenkel and MS behaviour to occur simultaneously. It not only considers the simultaneous sintering of clusters of particles with a distribution of sizes but also includes a distribution of pore sizes and the formation of necks between particles with different radii through the ξ factor with no adjustable factor.

The neck forming ability, ξ, depends on the shape and size distribution of the particles. If $\xi=1$ there is no mixing of particles of different sizes. When ξ is a function of r particles of different sizes are allowed to form necks, as illustrated in Figure 1, a fact that is corroborated by the results shown in Figure 5. For glasses in which crystallisation does not occur, predictions can be made with the model for other temperatures. This fact is important from a practical standpoint because it allows for previous anticipation of sintering results from simple calculations.

Sintering kinetics of the real powder used here is slower though not far from the calculated kinetics of a monodispersed distribution containing only average sized particles. The model provides a tool to estimate the sintering kinetics of real glass powders for any size distribution and temperature thus minimising the number of laboratory experiments.

Stoichiometric cordierite glass

As shown in Figure 6 ground cordierite powder consisting of monodispersed particles having a 10^{-5} m or larger particle size (as an example) does not fully sinter at any temperature. This result is consistent with the findings of the TC-7 Committee. Therefore, to densify cordierite glass particle size has to be further reduced (which may however hinder powder flow into moulds) or a coarse powder subjected to high energy milling for very short times must be used to reduce N_s.[15]

Assumptions and problems

It should be kept in mind, however, that several assumptions were made throughout this article. For instance a sharp transition from the F to the MS regime had to occur at $\rho=0{\cdot}8$,[6] the irregular particle shape of the ground particles was taken as spherical, the shrinkage anisotropy and internal crystallisation originating from the particle surfaces were neglected and, finally, and most importantly, the residual porosity that remained even in those glasses did not crystallise. Thus, at first sight, the general ability of the models (and of our algorithm) to predict sintering with concurrent crystallisation is quite surprising. Let us now briefly discuss each of these assumptions.

Transition between F and MS sintering stages. The Frenkel equation is valid for monodispersed spherical particles in the initial stages of sintering (a small percentage of shrinkage). Indeed some authors found that it describes sintering up to about 5% shrinkage[26] while others found that it works up to ~10% shrinkage.[27] The reasons for this difference are not clear but we took this upper bound for convenience (we plan to test this assumption further in the near future). The MS equation, on the other hand, should be valid for isolated, identical, spherical pores in a glass matrix (theoretically for $\rho>0{\cdot}9$[27]).

In this paper, for each particle size the passage from the Frenkel to the MS regime occurs when $\rho_F(r,t_{0{\cdot}8})=0{\cdot}8$ is reached. The pore radius a_0 in Equation (2) was adjusted to guarantee a continuous $\rho(r,t)$ function at $t=t_{0{\cdot}8}$. This adjustment was achieved by first computing $t_{0{\cdot}8}$ with Equation (1b), then calculating a_0 with the integrated version of Equation (2) at time $t=t_{0{\cdot}8}$. This procedure allows one to calculate the densification curve smoothly from the initial density of the compact to full densification; however, it assumes that the F model is valid up to $\rho=0{\cdot}8$ and that the MS model then suddenly takes over. We believe this is a reasonable approximation but it must be justified *a posteriori*, i.e. from a comparison between experiment and theory.

Particle geometry. The Frenkel equation was derived for monodispersed spherical particles in the initial stages of sintering. However, in most practical situations as in this article, we use irregular (ground) particles. Cutler[28] long ago demonstrated that irregular particles of soda–lime–silica glass sinter about five times faster than spheroidised particles of the same glass. This effect clearly depends on how the actual particle shape departs from the spherical. It is reasonable to expect that the particle shape has a significant effect on sintering only during the Frenkel stage since, in these early stages, necks begin to form and the original shape (radius of curvature) of the particles is still conserved. Within any given particle, ground particles have surfaces with a variable radius of curvature. Hence the initial (Frenkel) kinetics of sintering is determined by the distribution of different contacts formed among them. There is no memory of the original particle shape at the MS stage; hence no shape effect is expected there.

Shrinkage anisotropy. Although the effect of particle shape on sintering kinetics is not entirely clear, it is an experimental fact that sintering anisotropy depends on the anisotropy of the particles and their arrangement in the axial and radial directions before sintering.

In our previous article on irregular polydispersed particles[14] we found a marked sintering anisotropy. Figure 8, reproduced from that work, shows the axial and radial fractional shrinkage for all temperatures tested as a function of the reduced time. A marked anisotropy is evident with radial shrinkage about 25% higher than axial shrinkage. We assign that anisotropy to a geometrical rearrangement of the particles during uniaxial pressing. The flat sides of the irregular particles tend to align horizontally, leaving the acute ends (of high curvature) pointing radially. This is equivalent to the treatment performed by Giess *et al.*[2] However, Giess[29] found that even spherical cordierite particles exhibit anisotropy during sintering, concluding that the effect was due to a difference in radial and axial compaction of the particles. Despite the anisotropy, however, Figure 7 shows that both sintering curves followed a unique 'master curve' when plotted against the reduced time $\gamma t/\eta$.

Crystallisation towards the volume. Considering the competition between sintering and crystallisation, and density changes due to glass crystal phase transformations, the final density is given by

$$\bar{\rho} = \rho_c \left[\left(1 - \sum_p \alpha_v^p \right) + \sum_p \alpha_v^p \frac{\rho_p}{\rho_c} \right] \tag{13}$$

where

$$\alpha_v^p = \sum_r \alpha_{v,r}^p \tag{14}$$

Density changes due to crystallisation depend on the density of each crystalline phase. In some exceptional circumstances it may also be that, while one crystalline phase is denser than the glass, a concurrent crystalline phase has a lower density than the glass, producing a slight overall effect on density. Equations (10a) and (10b) are important when it is necessary to control the crystallised volume for instance to produce sintered glass ceramics.

Residual porosity

A recurrent problem in viscous flow sintering is residual porosity. The results of several authors, including our own, show that it is very difficult to achieve full densification even in the absence of crystallisation. In our case, with the noncrystallising alumino-borosilicate glass, about 4% of closed pores always remained in the glass regardless of the sintering temperature.

Mackenzie & Shuttleworth[10] extended their analysis to include the effects of applied pressure or gas trapped in the pores by including another term in the energy balance representing the mechanical work done by the pressure. They considered the case of both soluble and insoluble gas. In the latter case the bubble shrinks until the pressure of the glass equals $P=2\gamma/r$ where P is the capillary pressure driving sintering and r the radius of the bubble. If, at the moment when the pore becomes a closed sphere, the radius is a_0 and the pressure is P_0, then the equilibrium size of the bubble will be $r_{eq}^2 = P_0 . a_0^3/2\gamma$.

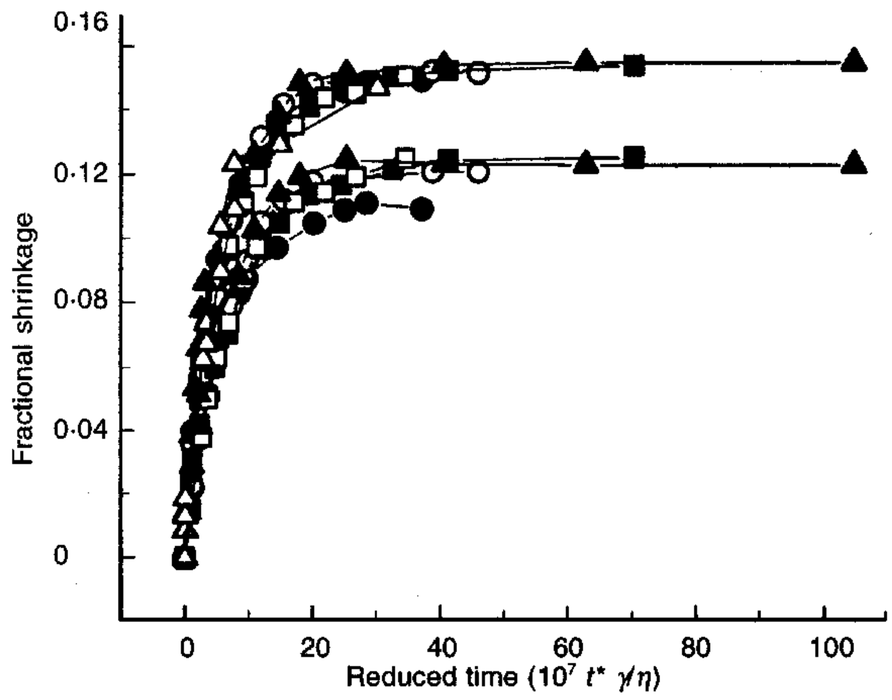

Figure 8. *Fractional height and diameter shrinkage for all temperatures used in Ref. 14*

● 959 K ○ 966 K ■ 980 K □ 989 K ▲ 999 K △ 1017 K

This problem is not taken into account in our equations. Water vapour and air (particularly N_2), for instance, have low solubility in silicate glasses. As described by Gaberer *et al*[30] for soda–lime–silica glass, water, nitrogen and carbon oxides (CO, CO_2) are released from the surface and volume of the sintering particles with a dynamics that depends upon the particle sizes. Adsorbed gases on particle surfaces are eliminated at low temperatures but gases dissolved inside the glass are released less easily by bigger particles. At the same sintering temperature, larger particles continue releasing these types of gases later. Additionally, crystallisation may induce gas release due to the different solubility of gases in the crystalline and vitreous phases. These gases may increase the porosity of the compact if they emerge during sintering.

A practical solution to avoid or minimise residual porosity is to sinter in a vacuum or in an atmosphere of soluble gas. For silica glass, for instance, it is best to sinter in helium.[12] However, in most cases this method may not be economically viable on an industrial scale. Another interesting solution may be to carefully adjust the particle size distribution so as to achieve the best packing and green density, starting with very small open pores, which will then be even smaller at the end of sintering.

Conclusions

Despite the complexity of the problem dealt with herein namely the sintering of polydispersed irregular particles with concurrent crystallisation, and the simplifying assumptions involved, we found good agreement between experiment and model. Even for some systems that include additional complicating factors such as pre-existing surface crystals, needle shaped crystalline phases or inclusions, which are very difficult to include in the mathematical equations, the calculations can still be useful to optimise thermal treatments.

Working windows constitute a new tool for experimental design through which porosity and crystallinity can be controlled. These windows can be calculated for mono and polydispersed crystallising glass powders. The example given shows that short, high temperature processes produce highly sintered compacts with low porosity and low cristallinity and vice versa.

The problem of residual porosity deserves special attention. Although the model discussed here considers the effect of surface crystallisation as a densification inhibitor, it does not consider the effect of entrapped air and degassing during sintering.

Finally, it should be stressed that throughout this paper, we have assumed that the specimens are heated at infinitely high heating rates. In some situations, however, both sintering and crystallisation may occur concurrently on the heating path before the sample reaches the chosen annealing temperature. This problem will be discussed in Part 2 of this article, submitted to this same journal.

Acknowledgements

This work was funded the Consejo Nacional de Investigaciones Científicas y Técnicas (Argentina), CNPq, PRONEX and FAPESP (Brazil). We also acknowledge R. Müller for his valuable suggestions.

References

1. Rabinovich, E. M. Preparation of glass by sintering. *J. Mater. Sci.*, 1985, **20**, 4259.
2. Giess, E. A., Fletcher, J. P. & Herron, L. W. Isothermal sintering of cordierite-type glass powders. *J. Am. Ceram. Soc.*, 1984, **67** (8), 549.
3. Chiang, Y. M., Birnie, D. P., III & Kingery, W. D. Single phase sintering. In *Physical ceramics. Principles for ceramic science and engineering*. 1997. John Wiley & Sons Inc, New York. Pp 392–8.
4. Van de Vorst, A. Numerical simulation of viscous sintering by a periodic lattice of a representative unit cell. *J. Am. Ceram. Soc.*, 1998, **81**(8), 2147.
5. Exner, H. E. & Giess, E. A. A stereology-based equation for isotropic shrinkage during sintering by viscous flow. *Science of sntering 7th*. 1989. Plenum Press, New York. P 73.
6. Müller, R. On the kinetics of sintering and crystallization of glass powders. *Glastech. Ber. Glass Sci. Technol.*, 1994, **67C**, 93.
7. Gutzow, I., Pascova, R., Karamanov, A. & Schmelzer, J. Kinetics of surface induced sinter crystallization. *Proc. Fifth Int. Otto Schott Colloquium*, Jena. 1994. P 81.
8. Zanotto, E. D., Prado, M. O. & Fredericci, C. Sintering with concurrent crystallization of monodispersed and polydispersed glass particles. Part 2. Non-isothermal treatments. *XIX Int. Congr. Glass Invited Volume*, 19–27. To be published in *Phys. Chem. Glasses*, 2002.
9. Frenkel, J. Viscous flow of crystalline bodies under the action of surface tension. *J. Phys. (USSR)*, 1945, **9** (5), 385.
10. Mackenzie, J. K. & Shuttleworth, R. A phenomenological theory of sintering. *Proc. Phys. Soc. (Lond) B*, 1949, **62**, 833.
11. Cutler, I. B. Sintering of glass powders during constant rates of heating. *J. Am. Ceram. Soc.*, 1969, **52** (1), 14.
12. Scherer, G. W. Sintering of gels. In *Sol-gel science and technology*. 1989.Edited by M. A. Aegerter, M. Jafelicci & E. D. Zanotto. World Scientific Publishing Co. Pte. Ltd., New Jersey. Pp 221–56.
13. Gutzow, I. & Schmelzer, J. The viscosity of glass forming melts. In *The vitreous state. Thermodynamics, structure, rheology and crystallization*. 1995. Springer, Berlin. Pp 32–40.
14. Prado, M. O., Zanotto, E. D. & Müller, R. Model for sintering polydispersed glass particles. *J. Non-Cryst. Solids*, 2001, **279**, 169–78.
15. Müller, R., Zanotto, E. D. & Fokin, V. M. Surface Crystallisation of silicate glasses: nucleation sites and kinetics. *J. Non-Cryst. Solids*, 2000, **274** (1–3), 208–31.
16. Prado, M. O., Fredericci, C. & Zanotto, E. D. Concurrent sintering and crystallization of soda-lime-silica glass spheres. In preparation, 2000.
17. Weinberg, M. C. Surface nucleated transformation kinetics in 2- and 3-dimensional finite systems. *J. Non-Cryst. Solids*, 1991, **134**, 116–22.
18. Müller, R., Kirsch, M. & Lorenz, H. Surface crystallization a limiting effect of sintering glass powders. *15th Congress on Glass*, Leningrad, Vol.3. 1989. P 334.
19. Gutzow, I., Pascova, R., Karamanov, A. & Schmelzer, J. The kinetics of surface induced sinter crystallization and formulation of glass-ceramics materials. *J. Mater. Sci.*, 1998, **33** (21), 5265.
20. Audero, M. A., Bevilacqua, A. M., Messi de Bernasconi, N. B., Russo, D. O. & Sterba, M. E. Immobilization of simulated high-level waste in sintered glasses. *J. Nucl. Mater.*, 1995, **223**, 151.
21. Bevilacqua, A. M., Messi de Bernasconi, N. B., Russo, D. O. & Audero, M. A. In Immobilization of simulated high-level liquid wastes in sintered borosilicate, aluminosilicate and aluminoborosilicate glasses. M. E. Sterba & A.D. Heredia. *J. Nucl. Mater.*, 1996, **229**, 187.
22. Mazurin, O. V., Streltsina, M. V., Shvaiko-Shvaikovskaya, T. P., Leko, V. K. & Priven, A. I. *SciGlassTM 3.0*, Universal Information System on Glass Properties. scivision@delphi.com, http://www.scivision.com.
23. Diaz-Mora, N., Zanotto, E. D., Hergt, R. & Müller, R. Surface crystallization and texture in cordierite glasses. *J. Non-Cryst. Solids*, 2000, **273**, (1–3), 81–93.
24. Fokin, V. M. & Zanotto, E. D. Surface and volume nucleation and growth in TiO_2 cordierite glasses. *J. Non-Cryst. Solids*, 1999, **246** (1–2), 115–27.
25. Müller, R., Zanotto, E. D. & Fokin, V. M. Surface crystallization of silicate glasses: nucleation sites and kinetics. *J. Non-Cryst. Solids*, 2000, **274** (1–3), 208–31.
26. Clark, J. K. & Reed., J. S. Kinetic processes involved in the sintering and crystallization of glass powders. *J. Am. Ceram. Soc.*, 1986, **69** (11), 837.
27. Scherer, G. W. Viscous sintering of a bimodal pore-size distribution. *J. Am. Ceram. Soc.*, 1984, **67** (11), 709.
28. Cutler, I. B. & Henrichsen, R. E. Effect of particle shape on the kinetics of sintering of glass. *J. Am. Ceram. Soc.*, 1968, **51** (10), 604.
29. Giess, E. A., Fletcher, J. P. & Herron, L. W. Isothermal sintering of cordierite-type glass powders. *J. Am. Ceram. Soc.*, 1985, **68** (12), C328.
30. Gaber, M., Müller, R. & Hölland, W. Degassing phenomena during sintering and crystallization of glass powders. *Glastech. Ber. Glass Sci. Technol.*, 1998, **71C**, 353.